The Crystal Structure of 5-Aminouracil and the Ambiguity of Alternative Polymorphs[#]

Taylor A. Watts[a], Louise S. Price[b], Sarah L. Price[b], Sara M. Niederberger[a], Jeffery A. Bertke[a] and Jennifer A. Swift[a]*

[a]Department of Chemistry, Georgetown University, 37th and O Sts NW, Washington, DC 20057-1227, USA. [b]Department of Chemistry, University College London, 20 Gordon Street, London WC1H 0AJ, UK. *Correspondence email: jas2@georgetown.edu

[#]*This paper is dedicated to Meir Lahav and Leslie Leiserowitz, in honor of their 2021 Wolf Prize*

ABSTRACT

The nucleobase derivative 5-aminouracil (AUr, $C_4H_5N_3O_2$) is of interest for its biological activity, yet the solid state structure of this compound has remained elusive owing to its propensity to crystallize as aggregates of microcrystalline particles. Here we report the first single-crystal structure of AUr determined from synchrotron x-ray diffraction data. An early crystal structure prediction effort, which assumed that AUr was rigid in the isolated molecule optimized conformation, provided several poor matches to the simulated PXRD pattern. Revisiting these crystal structures, by periodic electronic level modelling (PBE-TS optimization) gave more realistic relative lattice energies, but a good match to the experimental powder pattern required using the experimental cell parameters. PXRD and Raman spectroscopy suggest that phase impurities may be present in the bulk crystallization product, though the identity of alternative polymorphs could not be confirmed on the basis of the data available. (1015 characters)

1. INTRODUCTION

The structure and information transfer processes in DNA and RNA polynucleotides are intimately dependent on the hydrogen bonding between complementary nucleobases. When incorporated into oligonucleotides, nucleobase derivatives can provide key insights into the chemical interactions that stabilize (or destabilize) higher order nucleic acid assemblies. One such derivative is 5-aminouracil (AUr) shown in Figure 1. In triplex-DNA assemblies, binding of a third DNA oligoneotide strand in the major groove typically requires an available purine (guanine or adenine),[1] since these units have sites available to facilitate hydrogen bonding. With its 5-amino group, AUr was the first pyrimidine derivative shown to recognize all four DNA nucleobases (guanine, adenine, thymine, cytosine), and thereby provide additional stabilization for triple helical [2] and potentially quadruplex DNA assemblies.[3] The biological activity of AUr has also been demonstrated in other contexts[4] as has its use as a reagent in the synthesis of other heterocycles.[5]

Despite the significant biological and theoretical interest in this compound, no experimental crystal structure of AUr has yet been reported, in part due to its propensity to deposit as microcrystalline aggregates. Price and coworkers[6] previously computed the crystal structure energy landscapes for many 5-substituted uracils including AUr and identified a number of common hydrogen bonding motifs across the series including polar and non-polar ribbons, sheets and 3-dimensional network assemblies. However, the crystal energy landscape of AUr presented a particular challenge in the series, since the relative lattice energies were very sensitive to the hybridization geometry of the 5-amino group. The low planarization barrier for amino groups is

generally known to complicate the application of molecular *ab initio* methods to nucleic acid bases.[7]

Here we revisited the crystallization of AUr both from solution and via sublimation. Consistent with previous reports, large single crystals of AUr were quite difficult to grow, however, single crystal synchrotron x-ray diffraction enabled the first structure solution of this compound. The structure obtained was among those previously computed, though the corresponding computed structure was $> 10\,kJ\,mol^{-1}$ higher than the global minimum and therefore not considered experimentally feasible.[6a] The experimental geometry now available provided motivation to revise the estimated lattice energies. Powder X-ray diffraction on the bulk precipitated material and Raman spectroscopy on individual crystalline aggregates indicate that small quantities of at least one other polymorph may be present, which is consistent with thermodynamic plausibility of related computer-generated crystal structures.
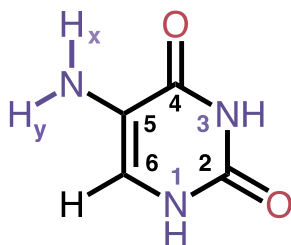

Figure 1. Molecular structure of 5-aminouracil in its most stable tautomeric form.

2. RESULTS AND DISCUSSION

AUr Growth and Structure Determination. In revisiting the crystallization of AUr using slow-evaporation methods from a variety of solvents and solvent-free sublimation methods, we again found that microcrystalline aggregates formed under essentially all conditions (Figure 2A). The largest microcrystals were obtained from 1:1 acetonitrile:water and aqueous solutions, though

smaller individual crystals could be obtained from sublimation. The bulk material obtained under these various conditions had a similar powder X-ray diffraction pattern, though some low intensity diffraction lines were present in some patterns but absent in others (Figure 2B). Heating under DSC conditions showed no thermal events below 300°C (Figure S1).
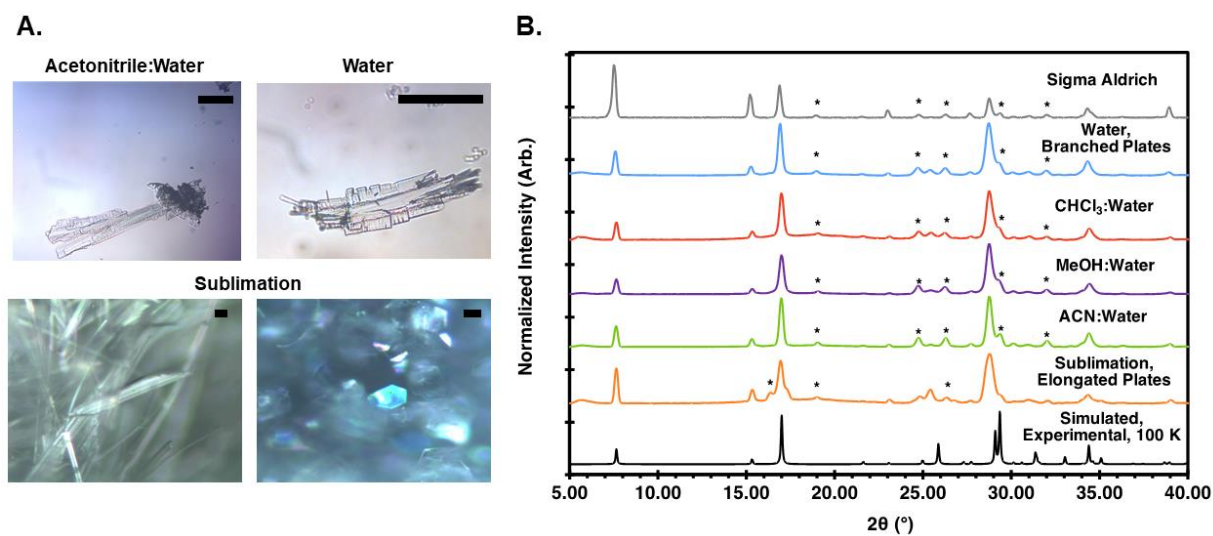

Figure 2. (A) Micrographs of AUr crystals grown from slow evaporation of 1:1 acetonitrile:water and water, and via sublimation. Scale bar = 100 µm (solution grown crystals) and scale bar = 10 µm (sublimation). (B) Room temperature PXRD patterns of AUr. (grey) Commercial material; Material obtained by slow evaporation from (blue) water, (red) 1:1 chloroform:water, (purple) 1:1 methanol:water and (green) 1:1 acetonitrile:water; (orange) Material obtained by sublimation. (black) Pattern simulated from the Pna2$_1$ single crystal structure determined from synchrotron data. Black asterisks indicate low intensity diffraction lines that do not appear in the simulated pattern.

Synchrotron diffraction data collected on AUr single crystals obtained from both 1:1 acetonitrile:water and sublimation enabled structure determination. Both data sets yielded the same Pna2$_1$ structure. The better of the two data sets refined to a cell with $a = 23.105(7)$, $b = 3.6041(11)$, $c = 5.8384(18)$ Å and $vol = 486.2(3)$ Å^3 and a R$_w$ = 6.06%. The other had similar cell parameters and a slightly higher R$_w$ = 6.99% (Table S1). There was no evidence of molecular disorder in either data set, and the quality of the data was sufficient to determine the H atom positions of the 5-amino group based on electron densities in the difference maps. Two views of

the structure are shown in Figure 3. AUr molecules assemble into 1-dimensional polar hydrogen bonded ribbons formed from N1-H…O2 and O2…H-N3 (blue dashed lines). Face to face π stacking of parallel ribbons along the *b*-axis creates dense polar layers in the (100) plane. When viewed down the *a*-axis, the ribbon directions in adjacent planes are shown to criss-cross at an angle of approximately 63°. Adjacent layers are connected by hydrogen bonds between N5-H…O4 (black dashed lines). Since the ribbon direction alternates between [011] and [01-1] in adjacent layers, any individual ribbon hydrogen bonds to ribbons in the adjacent layers above and below.

Since the H atoms of the 5-amino group could be located in the difference maps, the diffraction data provides experimental evidence for a slightly non-planar AUr geometry and for the existence of a weak intramolecular hydrogen bond between the 5-amino group and the adjacent carbonyl moiety. The C5-N5 bond length (1.407 Å) is on the shorter end of what one expects for a pure sp^3 hybridized primary amine,[8] potentially indicating that the bond has some sp^2 character. Previous computational studies suggested a weak intramolecular hydrogen bond may be present,[6a, 9] which would force the 5-amino group to rotate out of the plane as well as create a small non-planarity in the ring. The C4-C5-N5-Hx torsion angle in the experimental structure (-29.17°) is much larger than the angle predicted by *ab initio* methods on the isolated molecule (14.6°[9a] - 17.4°[6a]). Similarly the C4-C5-N-Hy torsion angle in the experimental structure (-177.85°) is also much larger than the calculated geometry (144.5°[9a] - 143.1°[6a]). Confirmation of this intramolecular hydrogen bonding is notable because it suggests the O4 position has a reduced proton affinity relative to uracil.[9b, 9c] Given the observed geometry of the 5-amino group in the 100K structure, and the high-amplitude, low frequency mode for NH_2 pyramidalization in crystalline urea,[10] it seems possible that the experimental structure reflects an average over

significant dynamic variation in the amine geometry. Though it was not possible to collect single crystal synchrotron data at multiple temperatures, such an experiment could reveal some interesting albeit subtle structural changes.
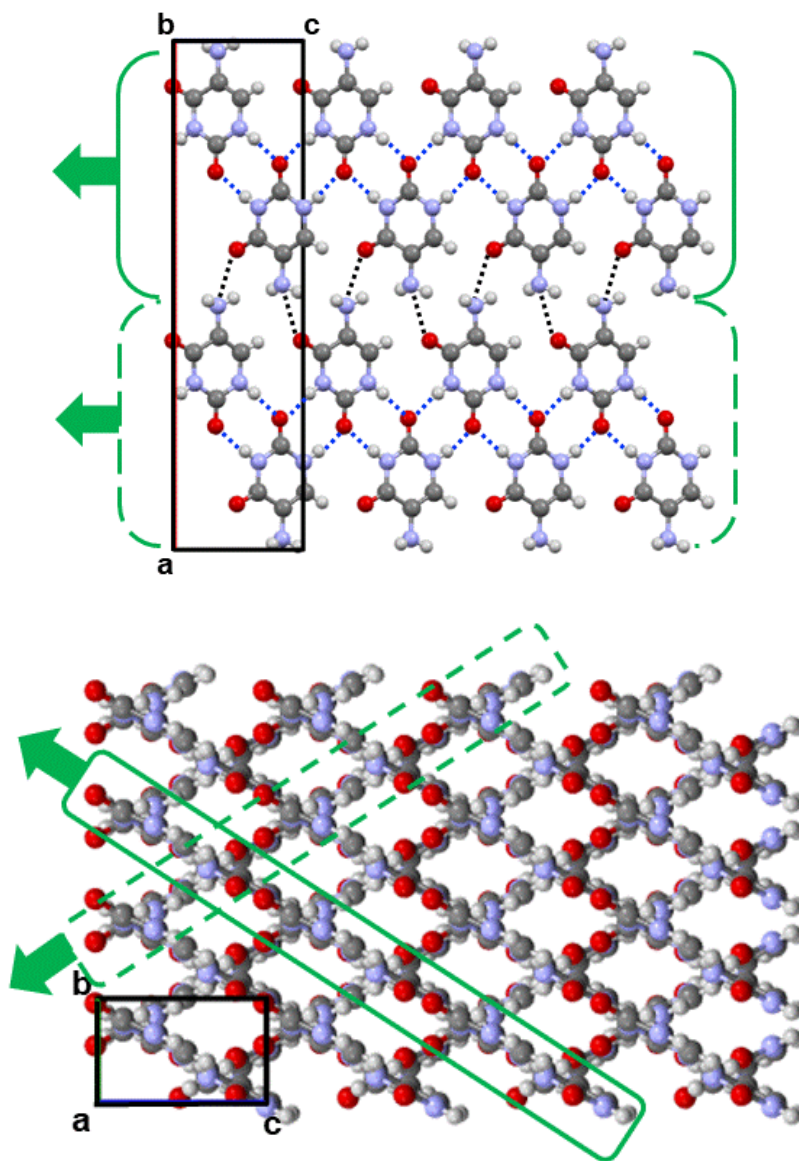

Figure 3. AUr structure determined from single crystal synchrotron diffraction data. (top) View down the *b*-axis shows the polar hydrogen bonded ribbon motif. Hydrogen bonds within each ribbon are shown in blue. Hydrogen bonds between ribbons in adjacent (100) layers are in black. (bottom) View down the *a*-axis shows how ribbons align in parallel to create dense (100) layers with face-face π stacks along the *b*-axis. The ribbon orientation in adjacent planes alternates

(green solid outline and green dashed outline), creating a criss-cross pattern and a net dipole along the *c*-axis. Atom colors: carbon (grey), oxygen (red), nitrogen (blue), hydrogen (white).

Computational Confirmation of Structure and Relative Energies. We set out to determine which of the previously computed structures corresponded to the experimentally determined form. In the 2008 Crystal Structure Prediction (CSP) study[6a] the computed fc35 structure was suggested as the best match to the experimental powder patterns in part based on the fact that it was one of the few ribbon structures within 5 kJ mol^{-1} of the estimated global minimum. Notably, the 2008 PXRD data and those obtained in the current study are not significantly different after accounting for the different radiation wavelength and other experimental details. The Similarity feature in Mercury[11] was used to compare the experimental structure against the entire set of previously computed AUr structures stored in the CPOSS database. Only one computed structure, au26 (RMSD$_{15}$ = 0.302Å), was found to have a 15 out of 15 molecule match when the default overlay settings were used. The next closest matches had only 11 out of 15 overlapping molecules. Typically, these structures showed a common layer structure with a symmetric ribbon motif, though one shared the common amino…carbonyl hydrogen bonding interface.

In the original CSP calculations which assumed a more pyramidal NH$_2$ geometry, the au26 structure was > 10 kJ mol^{-1} higher than the global minima, making it too high to be considered an experimentally feasible structure. With the development of periodic density functional methods which could optimize both the cell parameters and atomic coordinates[12] (unlike the original study which used rigid molecular geometries), it was possible to re-assess the relative energy of au26 and other select low energy computer-generated crystal structures. We considered the original global minimum structure (am91) as well as structures which also had a ribbon motif and a calculated energy within 5 kJ mol^{-1} (fc35 and bd74). To identify other CSP generated structures

that warranted reconsideration, the simulated PXRD pattern of each computed form was compared to the experimental synchrotron data using an established method based on Fidel.[13] The comparison yielded 3 additional structures with a reasonable score (bh14, fa95 and aj44). The CSP structure bh14 has the same polar symmetric ribbon and the same face-to-face ribbon stacking as the experimental structure, while fa95 and aj44 have a non-polar hydrogen-bonded ribbon motif. A feature[6b] of many 5-substitued uracils is the remarkable similarity in the PXRD patterns of polymorphs with polar and non-polar hydrogen bonded ribbon motifs (Figure S2). Packing diagrams of all alternative CSP polymorphs considered are shown in Figure S3.

The selected CSP generated structures were then optimized by periodic electronic structure methods. After PBE+TS optimization, the au26 structure was an even closer match to the experimental Pna2$_1$ structure (RMSD$_{30}$ = 0.196 Å RMSD$_{15}$= 0.150 Å). Curiously, the simulated PXRD pattern from this PBE optimized structure led to considerable shifts in the 2θ positions of some peaks, especially those with values for 2θ > 20⁰ (Figure 4, middle). The nominally 0 K static computed model actually has a larger cell volume than that observed at 100 K (492.66 vs 486.18 Å^3), and the magnitude of the differences in cell dimensions differs across the three principle axes such that the shifts from experimental positions vary with (*h,k,l*) distance. Re-optimization of the au26 structure with cell parameters fixed to match those in the 100K Pna2$_1$ structure shifted the diffraction line positions and the intensities into close agreement with the pattern simulated from the experimental structure (Figure 4, top). The agreement in line positions would be expected from the use of the experimental cell parameters; the optimization of the molecules within the fixed cell gave a reasonable molecular structure and intensities. The au26 structure is clearly the best match to the experimental form, though the temperature-dependent shifts in the PXRD patterns serve to illustrate one of the special challenges that can arise when attempting to match 0 K computed and

100 K – 298 K experimental PXRD patterns, particularly for crystals which may have highly anisotropic thermal expansion.[14]
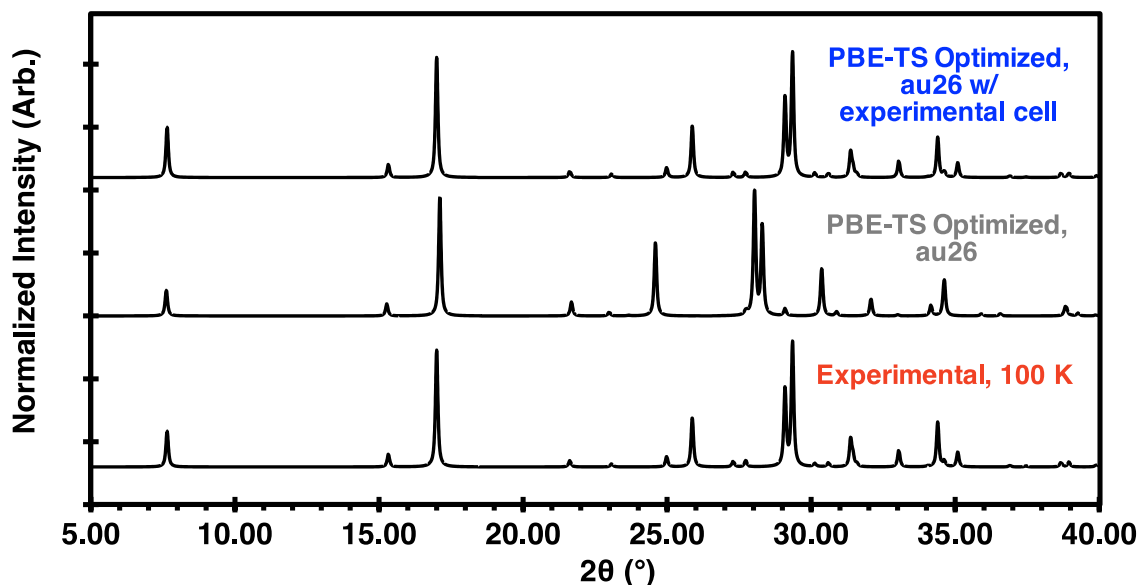

Figure 4. The PXRD pattern simulated from the 100K experimental Pna2$_1$ structure (bottom), compared against the PBE-TS optimized structure au26 (middle), and the lattice energy minimum when the unit cell is fixed at the experimental geometry (top).

When the PBE-TS optimized energies of the 7 other most likely low energy structures were considered against au26, there was a significant change in the relative energy ranking (Figure 5, Table S2). Single-point lattice energies calculated with the alternative MBD* dispersion correction altered the absolute PBE-TS energies slightly but did not change their relative ranking, supporting the assumption that the adaption of the amine geometry to the crystal packing was the main cause of the energy reranking. However, the PBE functional, which was the best that could be used, is known to suffer from delocalization error.[15] This affects the modelling of the N atom conformation and stability of polymorphs of 5-methyl-2-[(2-nitrophenyl)-amino]-3-thiophenecarbonitrile (ROY)[16] and dimethylamino-nitrochalcone[17] so our calculations are likely to have inaccurate amine geometries as well as cell volumes (Figure S4). The experimental au26

9

structure was only slightly (less than 1.2 kJ mol^{-1} Figure 5, Table S2) higher in energy than bd74 (which has the same layer structure and polar ribbons) and fc35 (which has non-polar ribbons). The smaller energy differences between au26 and other low energy structures are unquestionably more reliable than the rigid-molecule estimates in 2008, and are now consistent with au26 being the experimental structure. However, we note that the optimized computed structures do not include temperature or zero-point energy effects, which could further affect the relative energies.
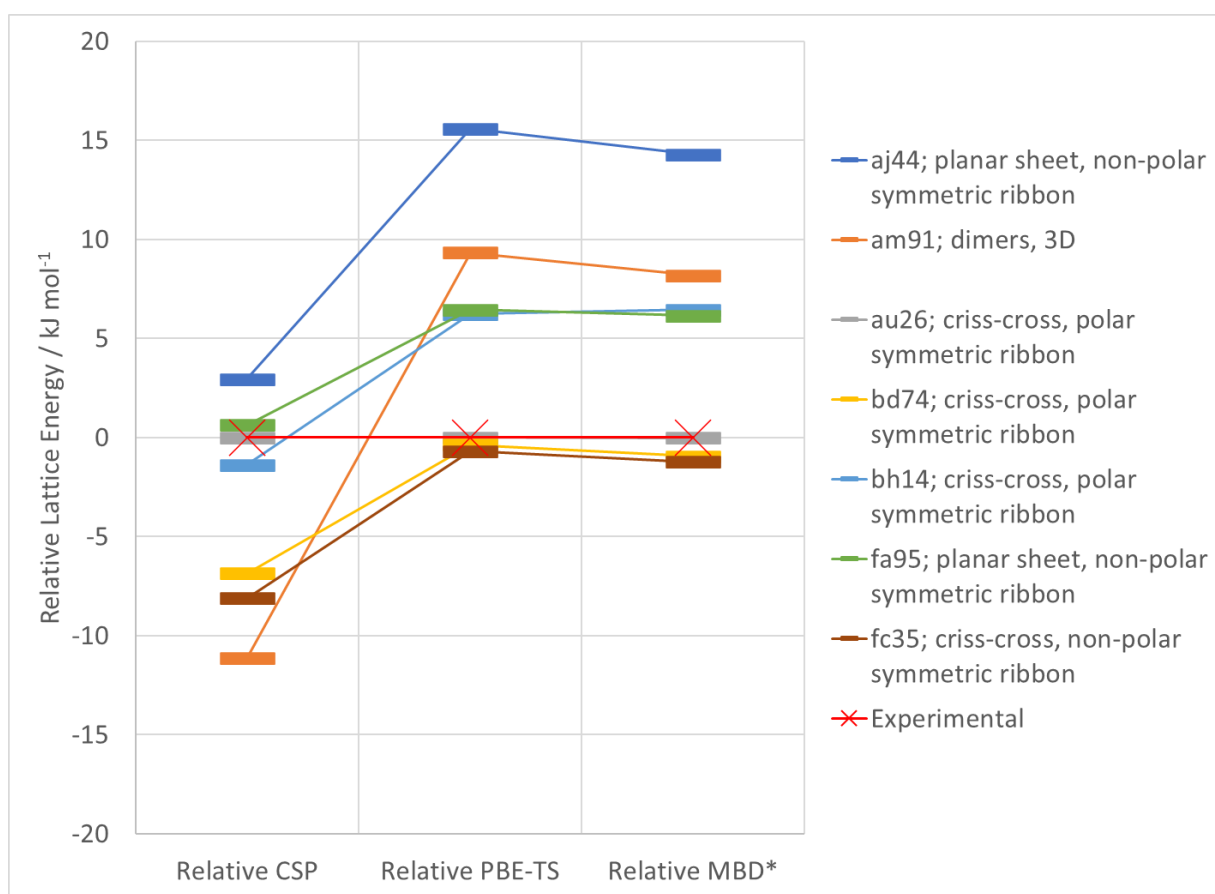

Figure 5. The lattice energy of selected CSP structures relative to the lattice energy minimum starting from the experimental structure for a variety of energy models. "Relative CSP" is calculated using the original CSP lattice energy model[6a] using the gas phase optimized molecular conformation; "Relative PBE-TS" is from structures optimized using PBE-TS, and "Relative MBD*" is from the use of the MBD* dispersion correction at the PBE-TS optimized structure.

Are there other identifiable polymorphs of AUr in the bulk samples? Comparison of

the simulated PXRD pattern generated from the .cif file accounted for all of the most intense

diffraction lines PXRD patterns of the bulk material obtained from the various growth conditions

(Figure 2B). Yet even in comparing the 100 K simulated $Pna2_1$ pattern and the room temperature

bulk experimental PXRD patterns, it is clear that some of the higher angle peaks shift due to

temperature differences. However, there are a few low intensity diffraction lines in some of the

bulk experimental PXRD patterns (e.g. at $2\theta = {\sim}16.5°, {\sim}19.2°$ and ${\sim}26.5°$ in the sublimed material)

that are not accounted for by the $Pna2_1$ structure. Some of the other computationally-generated

polymorphs considered have peaks at these positions. For example, am91 and fa95 have peaks at

$2\theta = 16.54°$ and $16.63°$, respectively, which is similar to the extra peak at $16.5°$ in the bulk

sublimed material. These same two CSP structures also have a peak at $2\theta = 18.99°$ and $18.87°$,

respectively, which appears in the sublimed material as well as in the commercial and solution

recrystallized materials. These structures have different uracil hydrogen bonding motifs to the

experimental structure. We are hesitant to attempt to match peaks with 2θ values greater than ${\sim}20°$,

given the potentially large changes in this region due to temperature. With only a few unique

peaks and the complicating effects of thermal expansion on the PXRD peak positions, it was

simply not possible on the basis of the data available to confirm the identity of the phase impurities

which are likely present in the bulk samples.

Raman micro-spectroscopy was also attempted here in an effort to characterize the phase

impurities in the bulk samples. Slow growth from aqueous solution yielded some of the largest

crystals, though often these were found as part of a larger aggregate of microcrystals. A typical

aggregate is shown in Figure 6 where several small crystals are seen attached to the sides of what

appears to be one larger central core crystal. The Raman spectrum of the center crystal (labeled

C) and those emerging from the sides (labeled A and B) show subtle differences in the region ~ 470-490 cm^{-1} as well as in the region just below 100 cm^{-1}. A previous DFT study on the isolated molecule[9a] assigned a vibration at 761 cm^{-1} to an N1-H stretch, and changes in that region could mean that polymorphs with very different N1-H local environments might be present. However, we observed some polarization dependence on the Raman spectra. In the absence of larger single crystals, it remains difficult to confirm whether aggregates contain different polymorphs or whether they are intergrowths of the same polymorph.
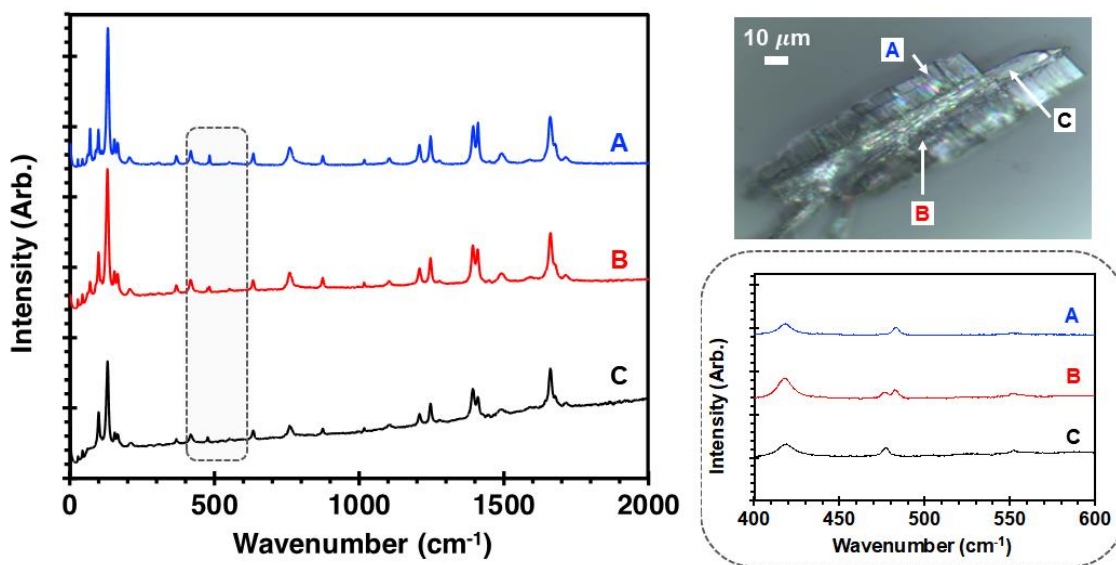

Figure 6. Micrograph of an AUr aggregate grown from aqueous solution and Raman spectra collected on different spots within the aggregate. The central crystal (C) has multiple crystals attached to two of its side faces. Raman spectra collected at different positions within the aggregate show slight differences in the number and position of peaks in the region between 450-500 cm^{-1}.

3. CONCLUSION

In this work, synchrotron radiation enabled the characterization of the first single-crystal structure of 5-aminouracil. This experimental polymorph was isolated from multiple crystal

growth methods and was identified as one of the computationally generated crystal structures assessed by Barnett et al. in 2008.[6a] Although we were able to structurally characterize only one polymorph of this compound, evidence suggests that additional polymorphs are likely present in the bulk growth products. This structural information will undoubtedly provide useful insights in understanding the effects of 5-substitution on uracil derivatives. This study illustrates the utility of cheap CSP studies which use rigid molecules, and also the challenges facing current computational modelling of the electronic and geometrical changes associated with the delocalization of -NH_2 groups and thermal expansion in the organic solid state. Nonetheless, the energetic competitiveness of different crystal structures provides evidence for the variety of hydrogen bonding interactions afforded by the AUr molecule that has made it an important nucleobase derivative in novel oligonucleotide assemblies.

4. EXPERIMENTAL

Sample Preparation. 5-Aminouracil (AUr) was obtained from Sigma-Aldrich (≥98%) and used without further purification. Ultrapure 18.2 MΩ water from an Elga Purelab Flex system was for all aqueous growth solutions. Other solvents were obtained in high purity from Fisher and MilliPore Sigma. Crystallization was attempted from aqueous solutions at 25°C and 4°C (~1.0 mg/mL) and from 1:1 methanol:water, 1:1 acetonitrile:water, and 1:1 chloroform:water solutions (~0.5-1.0 mg/mL) at 25°C. Sublimation experiments were carried out on a either a hot plate or hot stage microscope at approximately 160 °C. Sublimed samples were prepared between two glass slides where the source and deposition substrates were separated by spacers 3.18 mm in height. Solution crystallization yielded agglomerates of microcrystals under nearly all conditions,

though apparent individual crystals could be isolated in some cases. The sublimed product was a colorless polycrystalline material with varying morphologies.

Sample Characterization. Optical micrographs were obtained on either an Olympus BX-50 polarizing microscope fitted with a Lumenera Xfinity 2.0 camera, an HCS302 optical hot-stage (INSTEC, Inc., Boulder, CO) and Xfinity Analyze software (Lumenera, Ontario) or on a Horiba LabRAM HR Evolution confocal microscope. The thermal properties of AUr obtained from various methods were evaluated using a TA Instruments model 25 Differential Scanning Calorimeter (DSC). DSC dehydration experiments were performed using 0.5-5.0 mg of as-grown material in hermetically sealed aluminum pans at a heating rate of 5.0 °C/min from 25-390 °C. Powder X-ray diffraction (PXRD) data were collected at room temperature using a DUO Apex X-ray diffractometer (Cu Kα radiation, 50 kV, 30 mA current). Lightly ground samples were placed in Kapton capillaries (Cole-Parmer, 0.0320" ID x 0.0340" OD, 12"L) with data obtained from 2θ = 5−50°. PXRD data were integrated using APEX-2 software and analyzed using Panalytical X'Pert Highscore Plus software.[18]

Single Crystal Structure Determination. The single crystal structures of individual AUr crystals obtained from 50/50 acetonitrile/water and sublimation were determined from 100K synchrotron x-ray diffraction data collected at ChemMatCARS Sector 15 at the Advanced Photon Source. Frames were collected using ϕ scans in a Bruker platform 3-circle goniometer with fixed chi equipped with a Dectris PILATUS 100 detector, λ = 0.41328 Å, an undulator beam, and a diamond [111] crystal and two mirrors (to exclude higher harmonics) in the beam path. Data collection and unit cell refinement were carried out with SMART and data reduction with SAINT. Single crystal

structures were solved by intrinsic methods and refined using full-matrix least-squares on F^2 using SHELXT-Version 2014/5 and SHELXL-2018/3 software. Non-hydrogen atoms were modeled anisotropically while hydrogen atoms were treated with a mixture of independent and constrained refinement parameters. The hydrogen atoms on the 5-amino group were located in the difference maps. The ring N-H distances were restrained to be 0.86 (esd 0.01 Å). The remaining hydrogen atom was included as a riding idealized contributor. CCDC deposition number: 2091811

Raman Spectroscopy. Raman spectra were collected using a Horiba LabRAM HR Evolution confocal microscope with a 532 nm laser and 1800 I/mm grading filter. The laser power was set to 100%. A 50x objective was used with an acquisition time of 30 s for 2x accumulations.

Computation. The CSP structures were used as starting points for the periodic DFT-D structure optimizations with CASTEP[19] ver. 19.1 (**Error! Reference source not found.**). These calculations used the PBE functional with the Tkatchenko-Scheffler dispersion correction,[20] for the potential energy surface, with the ultrasoft pseudopotential.[19] Using a plane wave cutoff of 800 eV, a k-point grid spacing of 0.10 Å^{-1}, and a fine grid-scale of 4.0, all structures were optimized to a force tolerance of 0.001 eV/Å. Single-point energy calculations were then performed on the PBE+TS structures using the range-separated multi-body dispersion correction (MBD*).[21]

5. Acknowledgements

6. References

[1] M. D. Frank-Kamenetskii, S. M. Mirkin, *Annual Review of Biochemistry* **1995**, *64*, 65-95.
[2] (a) V. S. Rana, D. A. Barawkar, K. N. Ganesh, *The Journal of Organic Chemistry* **1996**, *61*, 3578-3579; (b) V. S. Rana, K. N. Ganesh, *Organic Letters* **1999**, *1*, 631-634; (c) V. S. Rana, K. N. Ganesh, *Nucleic Acids Research* **2000**, *28*, 1162-1169; (d) D. A. Barawkar, K. N. Ganesh, *Bioorganic & Medicinal Chemistry Letters* **1993**, *3*, 347-352.
[3] G. Paragi, Z. Kupihár, G. Endre, C. Fonseca Guerra, L. Kovács, *Organic & Biomolecular Chemistry* **2017**, *15*, 2174-2184.
[4] (a) H. H. Smith, C. P. Fussell, B. H. Kugelman, *Science* **1963**, *142*, 595-596; (b) D. Campo, R. Samaniego, J. F. Giménez-Abián, G. Giménez-Martín, J. F. López-Sáez, S. M. Díaz de la Espina, C. De la Torre, *Biology of the Cell* **2003**, *95*, 521-526.
[5] R. M. Shaker, M. A. Elrady, K. U. Sadek, *Molecular Diversity* **2016**, *20*, 153-183.
[6] (a) S. A. Barnett, A. T. Hulme, N. Issa, T. C. Lewis, L. S. Price, D. A. Tocher, S. L. Price, *New Journal of Chemistry* **2008**, *32*, 1761; (b) R. C. B. Copley, S. A. Barnett, P. G. Karamertzanis, K. D. M. Harris, B. M. Kariuki, M. Xu, E. A. Nickels, R. W. Lancaster, S. L. Price, *Crystal Growth & Design* **2008**, *8*, 3474-3481.
[7] S. Y. Wang, H. F. Schaefer, *Journal of Chemical Physics* **2006**, *124*, 044303-044308.
[8] H. Szatyłowicz, T. M. Krygowski, P. Hobza, *The Journal of Physical Chemistry A* **2007**, *111*, 170-175.
[9] (a) M. Alcolea Palafox, G. Tardajos, A. Guerrero-Martínez, V. K. Rastogi, D. Mishra, S. P. Ojha, W. Kiefer, *Chemical Physics* **2007**, *340*, 17-31; (b) A. K. Chandra, T. Uchimaru, T. Zeegers-Huyskens, *Journal of Molecular Structure* **2002**, *605*, 213-220; (c) S. R. Whittleton, K. C. Hunter, S. D. Wetmore, *The Journal of Physical Chemistry A* **2004**, *108*, 7709-7718; (d) J. Sponer, P. Hobza, *The Journal of Physical Chemistry* **1994**, *98*, 3161-3164.
[10] S. C. Capelli, M. Fortsch, H. B. Burgi, *Acta Crystallographica Section A - Foundations of Crystallography* **2000**, *56*, 413-424.

[11]   C. F. Macrae, I. Sovago, S. J. Cottrell, P. T. A. Galek, P. McCabe, E. Pidcock, M. Platings, G. P. Shields, J. S. Stevens, M. Towler, P. A. Wood, *Journal of Applied Crystallography* **2020**, *53*, 226-235.

[12]   (a) J. Binns, M. R. Healy, S. Parsons, C. A. Morrison, *Acta Crystallographica Section B-Structural Science Crystal Engineering and Materials* **2014**, *70*, 259-267; (b) J. van de Streek, M. A. Neumann, *Acta Crystallographica Section B - Structural Science* **2010**, *66*, 544-558.

[13]   S. Habermehl, P. Morschel, P. Eisenbrandt, S. M. Hammer, M. U. Schmidt, *Acta Crystallographica Section B* **2014**, *70*, 347-359.

[14]   A. van der Lee, D. Dumitrescu, *Chemical Science* **2021**.

[15]   L. M. LeBlanc, S. G. Dale, C. R. Taylor, A. D. Becke, G. M. Day, E. R. Johnson, *Angewandte Chemie-International Edition* **2018**, *57*, 14906-14910.

[16]   J. Nyman, L. Yu, S. M. Reutzel-Edens, *CrystEngComm* **2019**, *21*, 2080-2088.

[17]   C. L. Hall, R. Guo, J. Potticary, M. E. Cremeens, S. D. Warren, I. Andrusenko, M. Gemmi, M. A. Zwijnenburg, H. A. Sparkes, N. E. Pridmore, S. L. Price, S. R. Hall, *Crystal Growth & Design* **2020**, *20*, 6346-6355.

[18]   T. Degen, M. Sadki, E. Bron, U. König, G. Nénert, *Powder Diffraction* **2014**, *29*, S13-S18.

[19]   S. J. Clark, M. D. Segall, C. J. Pickard, P. J. Hasnip, M. J. Probert, K. Refson, M. C. Payne, *Zeitschrift fur Kristallographie* **2005**, *220*, 567-570.

[20]   A. Tkatchenko, M. Scheffler, *Physical Review Letters* **2009**, *102*, 073005.

[21]   A. Ambrosetti, A. M. Reilly, R. A. DiStasio, A. Tkatchenko, *J Chem Phys* **2014**, *140*, 18A508.